
Proceedings Paper:
Blackburn, L.R. orcid.org/0000-0002-5889-2035, Gardner, L.J. orcid.org/0000-0003-3126-2583, Sun, S.K. et al. (4 more authors) (2020) Hot isostatically pressed zirconolite wasteforms for actinide immobilisation. In: IOP Conference Series: Materials Science and Engineering. THERAMIN 2020 conference: thermal treatment of radioactive waste, 04-05 Feb 2020, Manchester, UK. IOP Publishing .

https://doi.org/10.1088/1757-899x/818/1/012010

Hot Isostatically Pressed Zirconolite Wasteforms for Actinide Immobilisation

IOP Conf. Series: Materials Science and Engineering **818** (2020) 012010 doi:10.1088/1757-899X/818/1/012010

Hot Isostatically Pressed Zirconolite Wasteforms for Actinide Immobilisation

L R Blackburn[1], L J Gardner[1], S K Sun[1], E R Maddrell[2], M C Stennett[1], C L Corkhill[1], N C Hyatt[1*]

[1]Immobilisation Science Laboratory, Department of Materials Science and Engineering, University of Sheffield, S1 3JD, UK.
[2]National Nuclear Laboratory, Workington, Cumbria, CA14 3YQ, UK.

*n.c.hyatt@sheffield.ac.uk

Abstract. In order to demonstrate the deployment of Hot Isostatic Pressing (HIP) for the immobilisation of Pu stocks and residues, a series of active and inactive zirconolite formulations have been processed and characterised. In this instance, Ce, U, and Th have been applied as chemical surrogates for Pu^{4+}. A range of formulations targeting isovalent Zr^{4+} site substitution (*i.e.* to simulate $CaZr_{1-x}Pu_xTi_2O_7$) have been processed by HIP and characterised by powder X-ray diffraction, and scanning electron microscopy, in order to determine surrogate partitioning between the host zirconolite phase, and accessory phases that may have formed during the HIP process.

1. Introduction

The United Kingdom holds a stockpile of civil separated plutonium that is forecast to exceed 140 teHM (tonnes equivalent heavy metal), subsequent to the completion of domestic reprocessing operations [1]. Immobilisation of Pu within a ceramic matrix such as zirconolite, prototypically $CaZrTi_2O_7$, may be a suitable pathway to disposition. Zirconolite has demonstrated extensive chemical flexibility with regards to feedstock chemistry, and as such is the dominant actinide-bearing phase in the Synroc formulation, developed for the immobilisation of high level waste (HLW) [2]. Pu^{4+} may be accepted into solid solution through Zr^{4+} site, *i.e.* $CaZr_{1-x}Pu_xTi_2O_7$ [3]. The Ca^{2+} site has also been demonstrated to accommodate Pu^{4+} through the addition of a suitable lower valence charge balancing species such as Al^{3+} (*e.g.* $Ca_{0.9}Pu_{0.1}ZrTi_{1.8}Al_{0.2}O_7$) [4]. The preferred final wasteform for Pu would require a robust processing route, insensitive to feed chemistry, with high throughput and waste loading.

Hot Isostatic Pressing (HIP) utilizes the simultaneously application of high temperature and isostatic pressing (typically through the use of an inert medium such as Ar gas) to consolidate and sinter materials to near-theoretical density. The HIP process is insensitive to the chemical properties of the feedstock, and produces minimal secondary waste, and is therefore a good candidate thermal treatment for the immobilisation of Pu stocks and residues [5]. In the current work, we report laboratory scale trials for zirconolite wasteforms processed by HIP. In this instance, CeO_2, UO_2 and ThO_2 were employed as chemical surrogates for PuO_2.

2. Materials synthesis and characterisation

2.1. Materials synthesis

Zirconolites were batched from oxide precursors ($CaTiO_3$, ZrO_2, TiO_2, CeO_2, ThO_2, UO_2) targeting nominal stoichiometry $CaZr_{0.8}Ce_{0.2}Ti_2O_7$, $CaZr_{0.8}U_{0.2}Ti_2O_7$ and $CaZr_{0.8}Th_{0.2}Ti_2O_7$. Precursor materials were optimised for HIP according to our previous investigations considering zirconolite glass-ceramic wasteforms [6]. Materials were batched and homogenised by high intensity ball milling (400 rpm, ~ 40 min), with the addition of isopropanol as a milling agent. Powder cakes were dried and passed through a sieve to break up agglomerates. Materials were then calcined at 600 ˚C in air for 12 h (Ar gas was used in the case of $CaZr_{0.8}U_{0.2}Ti_2O_7$ in order to maintain U^{4+}), before being pressed into the walls of a HIP can (316 stainless steel), under ~ 1 t uniaxial pressure. The cans were then evacuated at 300 ˚C for a further 12 h until approximately 50 mTorr pressure was achieved. The HIP cans were then hermetically sealed and placed into a AIP 630-H HIP unit and consolidated at 1300 ˚C and 100 MPa for 4 h.

2.2. Materials characterisation

A portion of the bulk ceramic was cut free from stainless steel containment and prepared for microchemical analysis using a Hitachi TM3030 scanning electron microscopy (SEM), fitted with a Bruker Quantax Energy Dispersive X-ray Spectrometer (EDS) for compositional analysis. The sample was mounted in cold setting resin and polished to a 1 μm optical finish using incremental grades of diamond suspension paste. SEM analysis was undertaken with a 15 kV accelerating voltage, and a working distance of ~ 8mm. A specimen was also mechanically ground prior to powder X-ray diffraction analysis using a Bruker D2 Phaser, using Cu Kα radiation ($\lambda = 1.5418$ Å). This was fitted with a Lynxeye position sensitive detector. Data were acquired in the range $5^\circ \leq 2\theta \leq 80^\circ$, with step size 0.02˚.

3. Results

3.1. $CaZr_{0.8}Ce_{0.2}Ti_2O_7$

The HIPing process was successful in all instances, and an example of a canister pre and post-processing is displayed in Figure 1. Powder X-ray diffraction data for $CaZr_{0.8}Ce_{0.2}Ti_2O_7$ are displayed in Figure 2. Refinement of the powder diffraction profile determined that zirconolite-2M was formed as the major crystalline phase – these reflections are indexed by relevant (hkl) values. Reflections consistent with the zirconolite-4M polytype phase were also observed, noted by (002) and (008) supercell reflections at $2\theta = 7.8^\circ$ and $2\theta = 31.1^\circ$, respectively. The formation of the zirconolite-4M polytype is consistent with previous observations, with the incorporation of tetravalent species within the Zr^{4+} site [7,8]. A considerable inventory of perovskite (parent structure $CaTiO_3$) was also stabilised; the formation of accessory perovskite phases is commonly attributed to the partial reduction of Ce^{4+} to Ce^{3+} [7,9]. XANES data (not shown) confirmed that a considerable fraction of Ce^{4+} was reduced to the Ce^{3+} species. EDS spotmap analysis of the perovskite phase, in this instance, confirmed the partial retention of Ce. Microscopic analyses (Figure 3) were consistent with powder XRD data. Zirconolite-4M and perovskite were clearly identified, distinguished by variation in backscattered electron contrast; these phases were consistently enriched in Ce.

Figure 1. Photograph of HIP canister pre and post-processing at 1300 ˚C and 100 MPa for 4 h.

3.2. $CaZr_{0.8}U_{0.2}Ti_2O_7$

When targeting nominal stoichiometry $CaZr_{0.8}U_{0.2}Ti_2O_7$, zirconolite-2M was formed as the dominant U-bearing phase, as determined by powder X-ray diffraction (Figure 2). Weak reflections indicative of a $(Zr,U)O_2$ solid solution were also identified. An ancillary perovskite phase was evidenced by powder XRD data (diagnostic reflection 2θ = 33.1˚) however, this was not clearly identified by SEM analysis. The zirconolite-4M polytype was not observed to form, contrary to experimental design and previous observations by Vance *et al*. [8]. Furthermore, UO_2 did not appear to be fully accommodated within the zirconolite phase, inferred by reflections consistent with the cubic UO_2 structure present in XRD analyses; SEM observations confirmed that free UO_2 was distributed throughout the microstructure (Figure 4). The $(Zr,U)O_2$ solid solution appeared to form at the rim of undigested UO_2 relics within the microstructure.

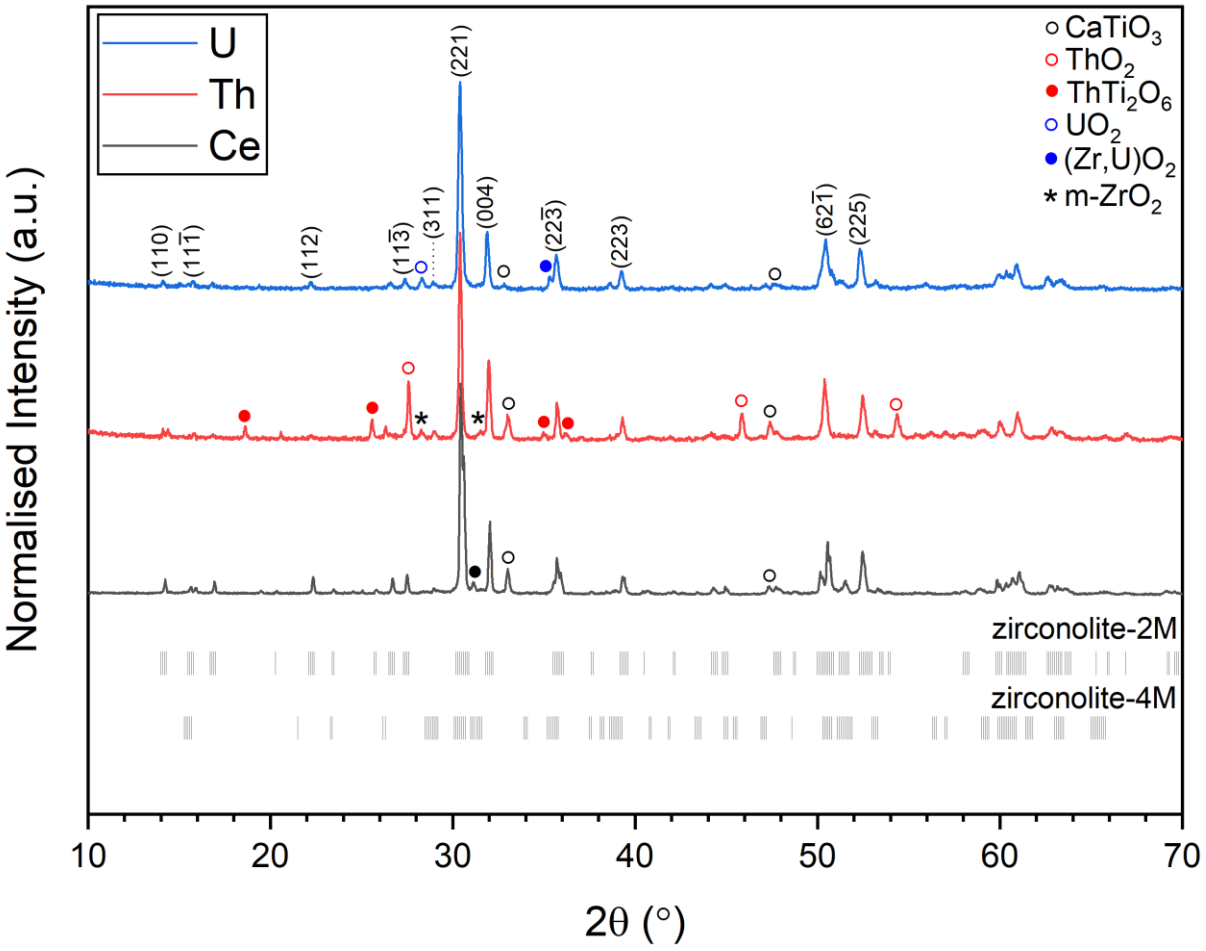

Figure 2. Powder X-ray diffraction data for $CaZr_{0.8}Ce_{0.2}Ti_2O_7$, $CaZr_{0.8}U_{0.2}Ti_2O_7$ and $CaZr_{0.8}Th_{0.2}Ti_2O_7$ processed by HIP at maximum temperature 1300 ˚C, at 100 MPa for 4 h. Zirconolite-2M reflections are labelled by (hkl) values; zirconolite-4M reflections are labelled by closed circles (●).

3.3. $CaZr_{0.8}Th_{0.2}Ti_2O_7$

Phase determination for $CaZr_{0.8}Th_{0.2}Ti_2O_7$ from powder XRD data are displayed in Figure 2. Diagnostic reflections consistent with zirconolite-2M were identified; these are labelled by appropriate (hkl) values. Intense (111) and (022) reflections, coherent with the fluorite structured ThO_2 phase, were clearly evidenced at 2θ = 27.5˚ and 2θ = 45.7˚, showing that ThO_2 was not fully incorporated within the zirconolite phase. This was confirmed by SEM analyses – see Figure 5. An ancillary perovskite phase was also clearly evidenced by powder XRD and SEM measurements. The zirconolite-4M polytype did not appear to form; a secondary thorutite phase, with ideal stoichiometry $ThTi_2O_6$, was stabilized. This phase was distributed around the rim of undigested ThO_2 within the microstructure as is illustrated in Figure 5.

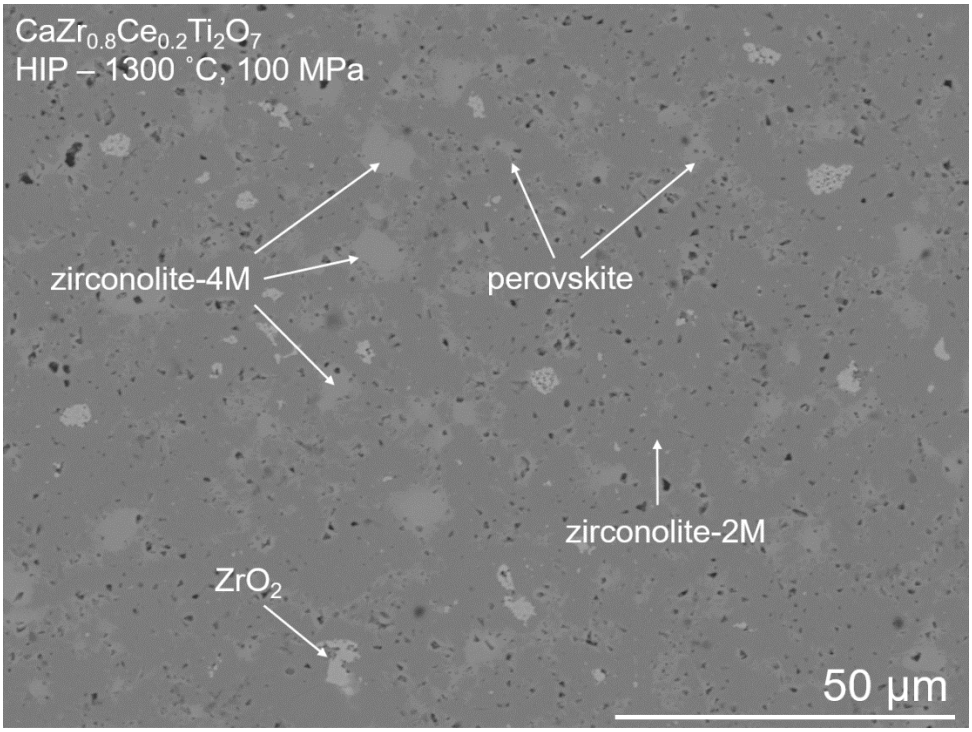

Figure 3. Representative backscattered electron micrograph of the $CaZr_{0.8}Ce_{0.2}Ti_2O_7$ microstructure formed by HIP at 1300 ˚C at 100 MPa

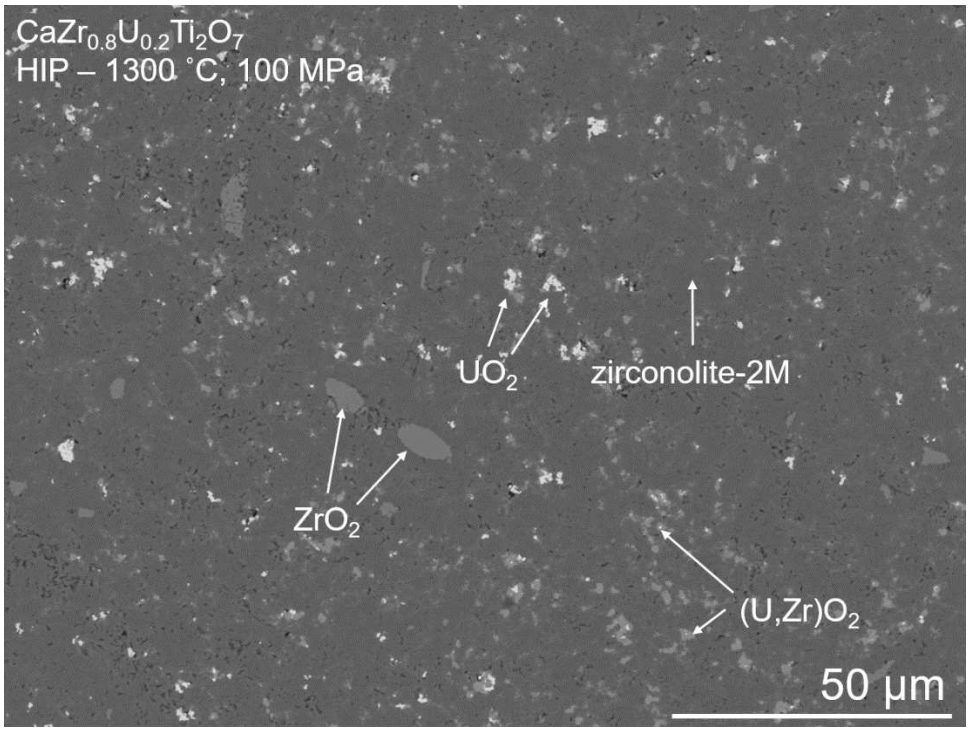

Figure 4. Representative backscattered electron micrograph of the $CaZr_{0.8}U_{0.2}Ti_2O_7$ microstructure formed by HIP at 1300 ˚C at 100 MPa

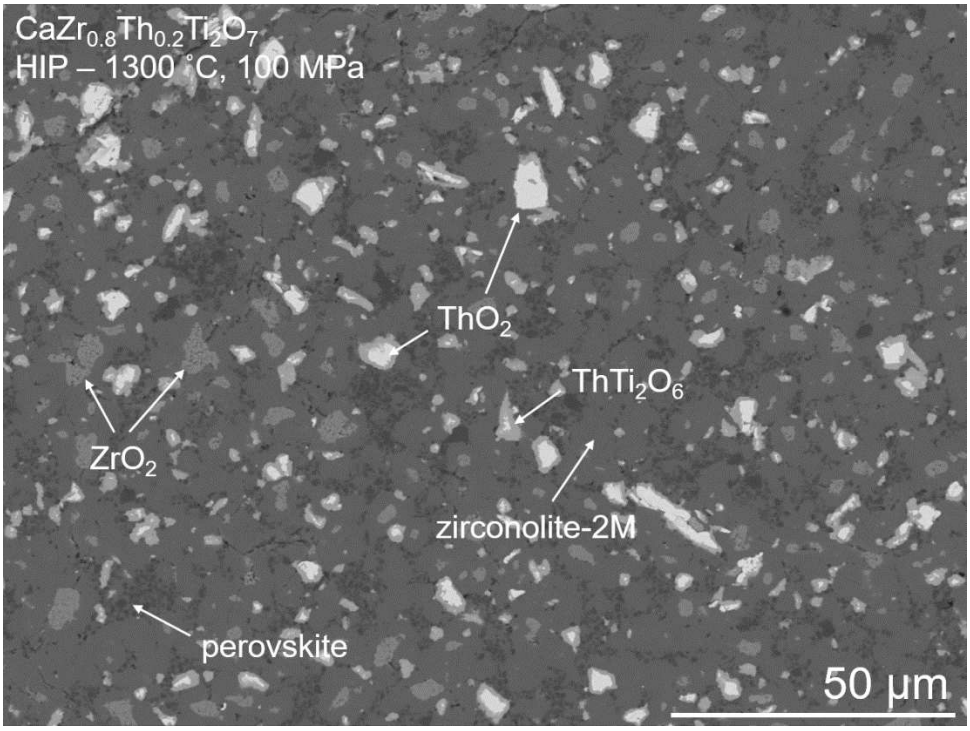

Figure 5. Representative backscattered electron micrograph of the $CaZr_{0.8}Th_{0.2}Ti_2O_7$ microstructure formed by HIP at 1300 ˚C at 100 MPa

4. Conclusions

Zirconolite wasteforms incorporated with CeO_2, UO_2 and ThO_2, chemical surrogates for PuO_2, have been processed by laboratory scale HIP. The processing parameters utilised a maximum temperature of 1300 ˚C, under an Ar pressure of 100 MPa; these conditions were held for a dwell time of 4 h. A mixture of zirconolite-2M and zirconolite-4M polytypes were observed when targeting nominal formulation $CaZr_{0.8}Ce_{0.2}Ti_2O_7$; a notable fraction of Ce-perovskite was also stabilised. The formation of perovskite is undesirable, due to inferior chemical durability with respect to the target zirconolite phase [10]. The crystallisation of zirconolite-4M was not observed in the case of $CaZr_{0.8}U_{0.2}Ti_2O_7$ or $CaZr_{0.8}Th_{0.2}Ti_2O_7$, due to the incomplete accommodation of UO_2 and ThO_2 within the zirconolite phase. The incorporation of UO_2 and ThO_2 within zirconolite stabilized secondary $(Zr,U)O_2$ and $ThTi_2O_6$ phases, respectively. The use of multiple surrogates may allow the imply the possible localization of Pu within a similar system. The reducing conditions imposed by the HIP environment may promote the formation of Pu^{3+}, and subsequent partitioning within the ancillary perovskite phase, decreasing the wasteform stability under hydrothermal conditions. These data demonstrate the need for careful phase design, in order to suppress the formation of deleterious accessory phases.

5. References

[1] Nuclear Decommissioning Authority (NDA), *Progress on Plutonium Consolidation, Consolidation, Storage and Disposition*, 2019.
[2] Ringwood A E, Oversby V M, Kesson SE, Sinclair W, Ware N, Hibberson W and Major A 2005 *Nucl. Waste Manag.* **2** 287.
[3] Begg B D, Day R A and Brownscombe A 2001 *Mat. Res. Soc. Symp. Proc*. **663** 1.
[4] Begg B, Vance E. and Conradson S. 1998 J Alloys Compd. **271–273**, 221.
[5] Maddrell E. 2012 Chem. Eng. Res. Des. **91** 735.
[6] Thornber S, Maddrell E, Stennett M C and Hyatt N C, 2016, in Proceedings of the Waste Management Symposium 2016, Phoenix, AZ, USA, 6 – 10 March 2016, 16581.

[7] Clark B M, Sundaram S K and Misture S T 2017 Sci. Rep. **7** 2.
[8] Vance E R, Lumpkin G R, Carter M L, Cassidy D J, Ball C J, Day R A and Begg B, 2002 J. Am. Ceram. Soc. **85** 1853.
[9] Begg B D and Vance E R, 1997 Mat. Res. Soc. Symp. Proc. **465** 333.
[10] McGlinn P J, Hart K P, Loi E H and Vance E R, 1995 Mat. Res. Soc. Symp. Proc. **353** 847.

Acknowledgement
We are grateful for financial support from the Nuclear Decommissioning Authority and EPSRC under grant numbers EP/201019X/1, EP/N017870/1 and EP/R511754/1. This research utilised the HADES/MIDAS facility at the University of Sheffield established with financial support from EPSRC and BEIS, under grant EP/T011424/1.